Top-down control of climate on long-term interactions between fires, tree-cover and soil erosion in a Mediterranean mountain, Corsica

Bérangère Leys, Lauriane Ribas-Deulofeu, Laurent Dezileau, Christopher Carcaillet

Quaternary Science Reviews 331 (2024) 108602

Contents lists available at ScienceDirect

Quaternary Science Reviews

journal homepage: www.elsevier.com/locate/quascirev

Top-down control of climate on long-term interactions between fires, tree-cover and soil erosion in a Mediterranean mountain, Corsica

Bérangère Leys [a,b,*], Lauriane Ribas-Deulofeu [a,c], Laurent Dezileau [d], Christopher Carcaillet [a,e,f,**]

[a] École Pratique des Hautes Études, Paris Sciences & Lettres University (EPHE-PSL), Paris, France
[b] Institut Mediterranéen de Biodiversité et d'Ecologie, Aix Marseille Univ, Avignon Univ, CNRS, IRD (IMBE), Aix-en-Provence, France
[c] Institute of Oceanography, National Taiwan University, Taipei, 106, Taiwan
[d] Laboratoire de Morphodynamique Continentale et Côtière, UMR CNRS 6143 M2C, Normandie Univ, UNICAEN, UNIROUEN, CNRS, M2C, 14000 Caen, France
[e] Université Claude Bernard Lyon 1, LEHNA UMR5023, CNRS, ENTPE, Villeurbanne, France
[f] Churchill College and Department of Plant Sciences, University of Cambridge, Cambridge, UK

ARTICLE INFO

Handling Editor: A. Voelker

Keywords:
Sediment
Granulometry
Biomass burning
Soil
Precipitation
Mediterranean

ABSTRACT

Fire is a potential significant driver of soil erosion in the Mediterranean area, as it results in the partial removal of vegetation and the alteration of organic matter, affecting soil structure and stability. The erosion of particle sizes is influenced by the intensity and duration of rainfall, regulated by disturbance regimes and vegetation cover. We hypothesize that, during the Holocene, high fire frequency and intensity under precipitation control may have contributed to soil erosion, while plant cover and composition could have mitigated it. This plant cover, in turn, might have been influenced by biomass burning. To test this hypothesis, we conducted a detailed analysis of sediments spanning the last 11,500 years from a small mountain lake, Corsica, situated in the black pine forest belt. The high temporal resolution analysis (~10 years per sample), used granulometry and loss-on-ignition as proxies for erosion and ecosystem productivity in both the lake and watershed, and fire and plant macroremains as fire and tree cover proxies, respectively. The correlation between particle size and the contents of organic or mineral matter with mean fire return intervals (FRI) revealed significant patterns. Long fire intervals were associated with more fine and coarse sands, whereas short mean FRI positively correlated with clay and, fine and coarse silt, along with higher total mineral and organic matter contents. These findings suggest that fires were more frequent when rain duration was sustained but runoff intensity was lower. Conversely, wildfires were less frequent during intense runoff periods (wetter climate). Unlike fire frequency, fire severity did not correlate with erosion, and tree cover and plant richness had minimal to no effect. The 8.2 kyr event was characterized by runoff transporting primarily coarse sands, i.e. a dry period with very intense rains. This suggests that the system is primarily top-down controlled by climate. Multimillennial erosion trends are influenced by fire frequency and precipitation regimes, whereas vegetation does not seem to have a mitigating effect on this process.

1. Introduction

Fires are potentially a major global threat to the environment and societies (Riera et al., 2007). They are enhanced by global warming, increasing drought, and reforestation (Rogers et al., 2020), with complex nexus to land uses (Moritz et al., 2014; Sayedi et al., 2024). In areas with long-lasting land use abandonment, the increasing woody biomass and tree-cover contribute to rise fire severity (Fernandez-Guisuraga and Calvo, 2023). In Europe, Mediterranean areas have a high fire risk due to landscape and climate conditions (Turco et al., 2018; Ruffault et al., 2020). Therefore, these areas are kettles of environmental threats and social concerns both linked to burning (Pausas and Fernandez-Muñoz, 2012; Moritz et al., 2014).

Soil loss and erosion are among the most important fire-related environmental issues (Shakesby, 2011; Stefanidis et al., 2022; Roshan and Biswas, 2023), notably in Mediterranean or arid areas due to vegetation removal and consumption of soil organic matter (OM). Soil OM plays a key role as a binder and reactor for mineral matter (MM),

* Corresponding author. École Pratique des Hautes Études, Paris Sciences & Lettres University (EPHE-PSL), Paris, France.
** Corresponding author. École Pratique des Hautes Études, Paris Sciences & Lettres University (EPHE-PSL), Paris, France.
E-mail addresses: berangere.leys@cnrs.fr (B. Leys), christopher.carcaillet@ephe.psl.eu (C. Carcaillet).

https://doi.org/10.1016/j.quascirev.2024.108602
Received 6 October 2023; Received in revised form 7 March 2024; Accepted 10 March 2024
Available online 28 March 2024

resulting in stable organo-mineral aggregates (Roshan and Biswas, 2023). Vegetation protects soil from erosion (Riera et al., 2007) although it remains complex to assess due to counter-effects (Nearing et al., 2004). Roots retain soil particles, and foliage attenuates the direct effect of water drops on the ground (Fernández-Raga et al., 2017). If not protected by vegetation, soil aggregates are disintegrated, and particles can be eroded according to their size and the rainfall regime following fires (Kinnel, 1976; Fernández-Raga et al., 2017). In forests, woody debris on the ground also attenuate runoff and erosion (Merganič, et al., 2023). If not protected by vegetation, smaller particles can be easily transported by gentle rains, while larger particles typically need intense rains and runoff to be transported, because of inertia and drag forces (Shi et al., 2013; Nguyen et al., 2016; Sun et al., 2021). In general, precipitation duration controls the total mass movement of MM, whereas rainfall intensity controls the selective transportation of particles according to their size (Sun et al., 2021).

The selected site, Creno lake (Corsica, west Mediterranean basin) presents sediments covering the past 18,000 years (Reille et al., 1997; Leys et al., 2014), but the present analysis will focus on the past 11,650 years (Holocene; Walker et al. 2009) characterized in this lake by permanent vegetation cover and fire occurrence: the site has indeed experienced changes in fire regimes (Leys et al., 2013), as well as in vegetation and fire-vegetation interactions (Leys et al., 2014). Fire regimes and vegetation cover are included in the analysis as potential direct or indirect drivers of erosion. The regional climate has also undergone variations (e.g., Bini et al., 2019; Lüning et al., 2019; Cisnero et al., 2021). While bedrock and topography can be considered fixed environmental factors since the last glaciation, sediment composition in MM and particle size are thus expected to have fluctuated significantly according to changes in precipitation, fire and vegetation, including tree cover or species composition (Fig. 1). We assume that changes in sediment granulometry is associated with periods of intense rain (more sands), longer rain (more MM), and gentle or Saharan "red" rain (more clays) (Fig. 1a). The chronology of the Saharan rain has been otherwise well established in Corsica by the sediment analyses of a supra-forest lake situated at 22 km to the southeast of the study site (Sabatier et al., 2020).

We hypothesize that during the Holocene, long-term soil erosion could result from higher fire frequency and severity, and that erosion could be mitigated by plant cover or composition, which would have changed according to biomass burning. Finally, the sediment granulometry would be linked to the precipitation regime. More intense rains transport more sands by runoff, while clay particle can only result from erosion from the watershed, Saharan air masses, or both. Indeed, Saharan air masses supply "red dusts" that are important clay and nutrients inputs in southern Europe (Loye-Pilot et al., 1986; Martinez-Cortizas et al., 2019). Long-distance inputs of dusts can alter the elementary and particles budget in Mediterranean-type mountains (Loye-Pilot and Morelli, 1988; Aciego et al., 2016). To test this general hypothesis, sediments must be analyzed at high temporal resolution, to establish accurate interactions between the ecosystem components, i.e., vegetation, fire and soil, to decipher which ones behaved as erosion drivers, and how.

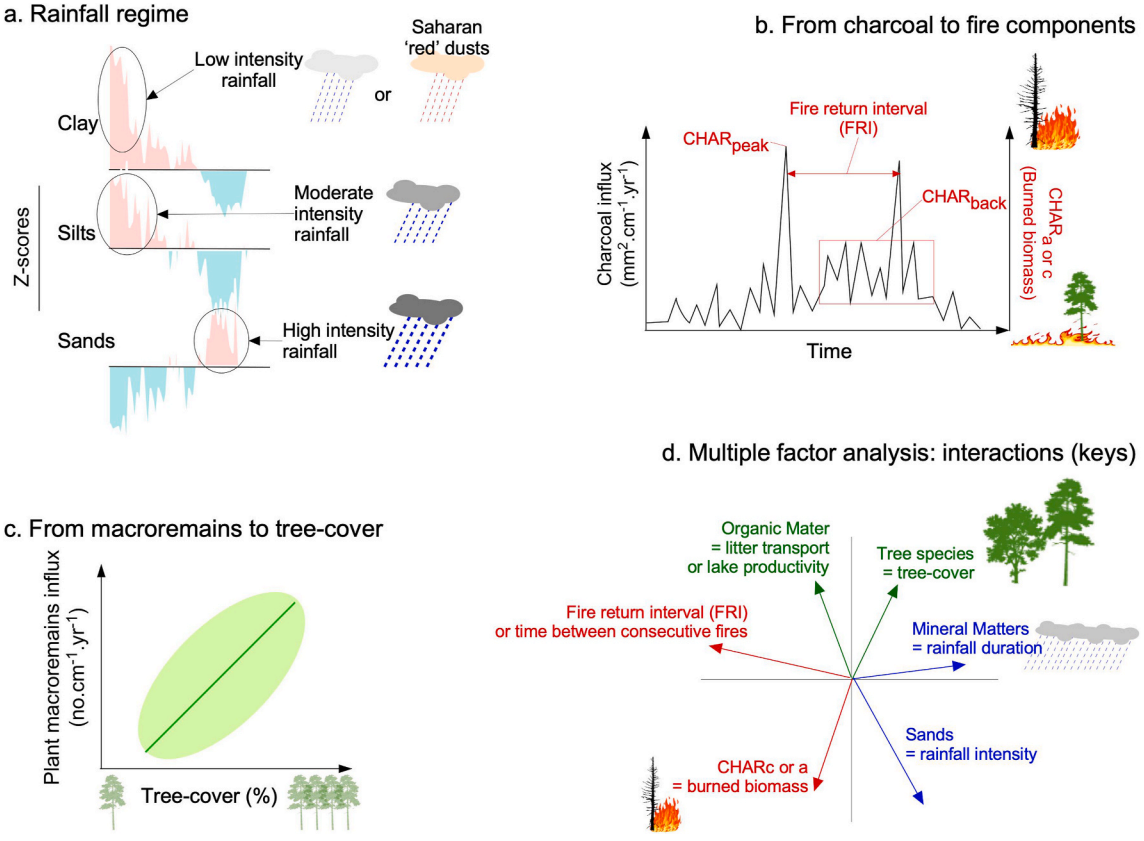

Fig. 1. Conceptual framework of the study. (**a**) The granulometry reflects the precipitation regime, where the ratio of sand:total input reflects intense rainfalls, and the clay:total input illustrates low intense rainfall or the contribution of Saharan 'red' dust; silts should represent an intermediate pattern of rainfall. (**b**) From charcoal counting to reconstruction of fire regime, where charcoal peaks represent fire events, time between two consecutive peaks is the fire return interval (FRI), the magnitude of charcoal peaks corresponds to fire severity ($CHAR_c$ or $CHAR_a$), and the background is the influence of extra-local fires ($CHAR_{back}$). (**c**) The tree-cover can be reconstructed based on concentration rates (or influx) of tree macro-remains. (**d**) Summary of key proxies and their interpretation on a bi-plot similar to multiple factor analysis.

2. Material and methods

2.1. Study sites

Creno lake (1310 m asl; 42°12′17″N, 08°56′45″E) is located in a west-facing slope of the Rotondo massif, western Corsica (Fig. 2 and S1). The 1.5-ha and 6.5-m deep lake is situated on a flat area on a narrow crest similar to a "horse saddle" (Fig. S1). It has no permanent inflow. Rainfalls are captured within a small catchment (~25 ha) peaking at 1511 m asl. The bedrock is based on monzonitic granite, that generates acidic and shallow cambisol with a loamy-sandy granulometry, and moder or dysmull humus (IFN, 2006).

Climate varies highly from site to site in Corsica due to an abrupt mountain relief (north-south ridges) and dominant westerly air masses supplying moisture. In the nearest weather station from Creno lake at 755 m asl, for the 1991–2020 period, the mean annual temperature was 11.8 °C, with mean monthly temperatures of 4.9 °C for the coldest month (January) and 20.1 °C for the warmest (August). Mean annual precipitation was 1181 mm, ranging from 98 mm during the growing season (P_{JJA}), and 379 mm in winter (P_{DJF}). The wettest month was typically November with more than 190 mm on average. Gams indexes (Michalet et al., 2020) for summer and winter are of 66° and 30°, respectively, characterizing a semi-arid (summer) to very-humid (winter) Mediterranean mountain climate. Between 1993 and 2020, the maximal daily precipitation was 92 mm day^{-1} on average, ranging from 52 mm day^{-1} (August 1998) and 133 mm day^{-1} (May 1994), which reveals a precipitation regime with high runoff and erosion power that can occur in any season.

Regarding vegetation, the lake is situated in the lower montane belt characterised by mixed forests of *Pinus nigra laricio* (Poir.) Maire (Corsican pine), *Fagus sylvatica* L. (beech), and *Abies alba* Mill. (white fir) with an understorey of *Genista corsica* (Loisel.) DC, *G. salzmannii* DC and tall heather species, mainly *Erica arborea* L. (Gamisans et al., 2000).

The onset of the Holocene (~11,650 cal year BP) was marked by a rapid treeline shift, the establishment of *P. laricio* woodlands with low species turnover, and a long-term increase in taxa richness as a result of successive expansions of broadleaved deciduous trees. Despite a mean fire-return interval (FRI) of 135 years during the Holocene, *P. laricio*-dominated woodlands persisted for several millennia, and fires likely played a functional role in these woodlands. The mean FRI of 135 years between fires correspond to a frequency of 7.5 fires per 1000 years (Leys et al., 2014), which is much lower than reported over the past two centuries in a study carried in central Corsica with 41 major fires per 1000 years (Badeau et al., 2024). This Corsican high frequency during the last 200 years matches the records in similar black pine forest in Spain (64 per 1000 years in Fulé et al., 2008), Greece (67 in Christopoulou et al., 2013), and Turkey (59 in Şahan et al., 2022).

2.2. Sampling

Parallel overlapping cores were extracted in 2009 from the deepest area of the lake, at a water depth of ~6 m using both a large Russian corer for the compacted sediment (starting at 20 cm under the water-sediment interface, ended up at about 7 m sediment depth), and a Kajak-Brinkhurst corer for the uppermost water-saturated sediments (about 30 cm depth) at the same coring point, before the Russian corer extraction.

Two parallel 7-m cores were sampled with the Russian corer in order to analyze sediments by avoiding the core section transitions where the device disturbed the sediment. One core was used for sedimentological analysis (present study), and the second one for the analysis of charcoal and terrestrial plant macrofossils (Table 1, details in Leys et al., 2013, 2014). The two parallel cores have been correlated based on sedimentary descriptions and charcoal concentrations, and with the Kajak-Brinkhurst core, to constitute a master-core of 695 cm in total from the water-sediment interface to the deepest collected sediment.

Table 1
Accelerator mass spectrometry (AMS) radiocarbon dating on plant remains (needles of *P. nigra laricio* or seeds of *Betula*) and bulk sediment.

Depth (cm)	Lab code	^{14}C years BP	Dated material
90–95	Poz-36753	1415 ± 30	Plant remains
175–180	Poz-36754	3360 ± 35	Plant remains
240–245	Poz-36755	4705 ± 35	Plant remains
355–360	Poz-38609	7740 ± 60	Plant remains
370–375	Poz-36803	8150 ± 50	Bulk sediment
385–390	Poz-38612	8350 ± 60	Plant remains
435–440	Poz-36758	9630 ± 50	Plant remains
495–500	Poz-36759	11,250 ± 60	Plant remains
526–531	Poz-36802	12,850 ± 80	Bulk sediment
580–585	Poz-36760	13,130±70	Bulk sediment
670–675	Poz-38611	14,430 ± 90	Bulk sediment

2.3. Isotopic dating

Isotopic radioactive measurements (^{210}Pb and ^{137}Cs) were used to build an accurate age~depth model for the upper sediments (Kajak-Brinkhurst core), and radiocarbon (^{14}C) for the longest and deepest cores. Dating of sedimentary layers was carried out using ^{210}Pb and ^{137}Cs methods on a centennial time scale. Both nuclides together with U, Th, and ^{226}Ra were determined by gamma spectrometry at the Géosciences Montpellier Laboratory. The 1-cm-thick sediment layers were sieved in order to obtain the fraction smaller than 1 mm. This material was then finely crushed after drying and transferred into small gas-tight PETP (polyethylene terephtalate) tubes (internal height and diameter of 38 and 14 mm, respectively), and stored for more than 3 weeks to ensure equilibrium between ^{226}Ra and ^{222}Rn. The activities of the nuclides of interest were determined using a Canberra Ge well detector and compared with the known activities of an in-house standard. Activities of ^{210}Pb were determined by integrating the area of the 46.5 keV photopeak. ^{226}Ra activities were determined from the average of values derived from the 186.2 keV peak of ^{226}Ra and the peaks of its progeny in secular equilibrium with ^{214}Pb (295 and 352 keV) and ^{214}Bi (609 keV). In each sample, the (^{210}Pb unsupported) excess activities were calculated by subtracting the (^{226}Ra supported) activity from the total (^{210}Pb) activity. Here, parentheses () denote activities. Activities of ^{137}Cs were determined by integrating the area of the 661-keV photopeak. Error bars on (^{210}Pbex) and (^{137}Cs) do not exceed 6%.

The depositional model was extended down the core using 11 calibrated ^{14}C dates measured by accelerator mass spectrometry (AMS) on plant macrofossils or on the total organic matter contents of bulk sediments when macrofossils were not sufficiently abundant (Table 1). The age~depth model was performed using Bacon R package (Blaauw and Christen, 2011), based on ^{210}Pb and ^{14}C dates reported in Table 1, with calibration of ^{14}C dates into calendar years (hereafter Cal BP) through IntCal 20 (Reimer et al., 2020) (Fig. 2). To test the robustness of the age ~ depth model, we compared it to the un-modelled ^{14}C chronology of Reille et al. (1997, 1999), and with the chronology of the seminal study published by Leys et al. (2014), which was found to be correlated at 0.9995.

2.4. Sedimentological measurements

The 7-m long core was sampled every 1 cm for sediment analysis, totalizing 677 samples, including 439 during the Holocene (11,650 cal BP to present) and 238 during the Lateglacial starting at 18,000 cal BP and ending with the Younger Dryas (12,900 to 11,650 cal BP; Walker et al., 2009), a cold period in the Northern Hemisphere.

The composition of sediment in terms of organic and mineral matter was determined through loss-on-ignition (LOI). Following sediment drying at 105 °C for 2 h, LOI was conducted at 550 °C for 1 h at 1-cm intervals along the core to assess the relative abundance of organic matter (sediment consumption) and the residues from ignition. Ignition

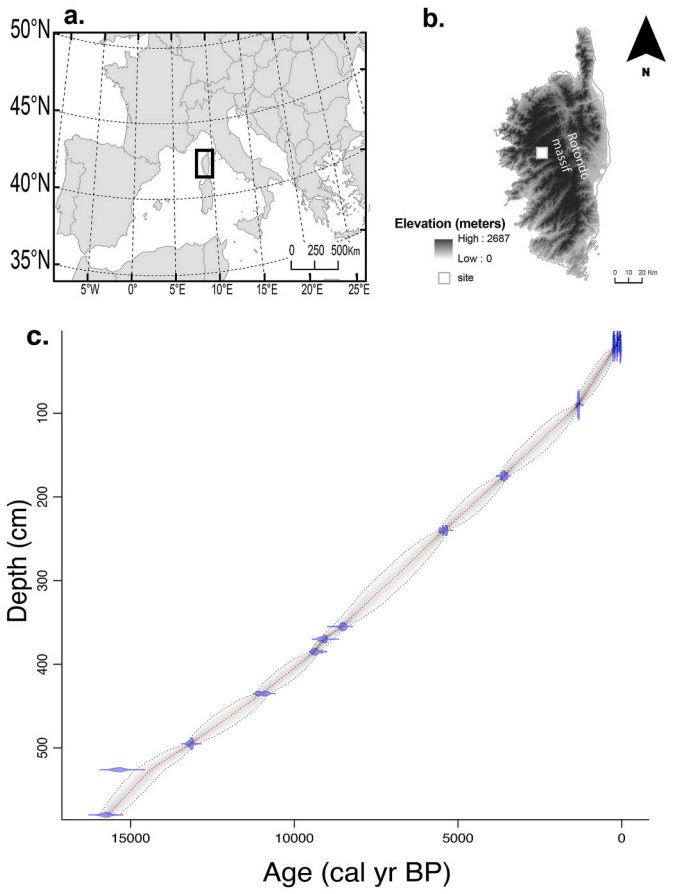

Fig. 2. (**a**) Location of Corsica within southern Europe, (**b**) Location of sedimentary records in Corsican mountains of the Rotondo massif, and (**c**) Age~-depth model for the Creno Lake core based on ^{210}Pb and ^{14}C dates, run on Bacon package of R cran.

residues are considered to be inorganic particles, such as silt, clay, and sand, originating from the watershed or, possibly, from aeolian activity, and referred to as mineral matter. LOI measurements were not taken in the top 20 cm of the core sequence due to the limited sediment volume caused by suspended sediment at the water-sediment interface.

For granulometric analysis, sediments were sieved wet at 2 mm. A laser particle sizer Coulter LS-230 was used equipped with an ultrasound probe to obtain granulometric fractions from 0.3 μm to 2 mm in diameter. Particles were classified in 92 intervals of diameter-class (Fig. S2) and grouped into 5 categories (Table 3) according to the usual classification (Day, 1965).

2.5. Charcoal-based fire reconstruction

For fire analysis, the core was sampled every 0.5 cm yielding 1400 contiguous 0.5-cm thick samples. Charcoal measurements included charcoal concentration per area, $CHAR_{conc}$ (unit: nb cm^{-3}) and charcoal accumulation rates, $CHAR_{area}$ (mm^2 cm^{-2} yr^{-1}) (Leys et al., 2013). The magnitude of $CHAR_{conc}$ or $CHAR_{area}$ at a fire event is a proxy for the area burnt or fire severity (Hennebelle et al., 2020).

Local fire episodes were inferred from the charcoal record using the decomposition approach, which separates the charcoal peaks $CHAR_{peak}$ and charcoal background $CHAR_{back}$ (Higuera et al., 2011). The $CHAR_{peak}$ is a proxy for local fire events because most charcoal particles are in situ produced (Clark et al., 1998; Ohlson and Tryterud, 2000; Lynch et al., 2004) in the absence of runoff mobilization from the catchment (Carcaillet et al., 2007). The $CHAR_{back}$ component is a proxy for the area burned in the near valleys of Creno Lake, but also probably during local frequent surface fires, which are assumed poorly productive in terms of charred particles and difficult to detect using the above numerical pipeline.

The abundance of charcoal ($CHAR_{conc}$ or $CHAR_{area}$) associated to a charcoal peak is a proxy for burned conifer forest areas or fire severity considering the distance of the burned area from the lake (Hennebelle et al., 2020), but this could be filtered by the riparian forest around the lake in dry conditions (Aleman et al., 2013). Today, there is no such riparian vegetation surrounding the mountain lake of Creno as well as around the other mountain lakes in Corsica.

Table 2
Variables used in the Multiple Factor Analysis (MFA).

Category	Data	Abbreviations	Units
Vegetation	Macroremains of fruits of *Betula*	*Betula*	pieces. $yr^{-1}.cm^{-2}$
	Macroremains of cones and needles of *Pinus laricio*	*Pinus laricio*	pieces. $yr^{-1}.cm^{-2}$
	Macroremains of leaves and seeds of *Fagus*	*Fagus*	pieces. $yr^{-1}.cm^{-2}$
	Rarefaction of all plant macroremains following Blarquez et al., (2013)	Rarefaction	No unit
Fire	Charcoal area accumulation rate	CHARa	$cm^2.yr^{-1}.cm^{-2}$
	Charcoal count accumulation rate	CHARc	pieces. $yr^{-1}.cm^{-2}$
	Fire return interval	FRI	Years
Sediment	Concentration of mineral matter from loss-on-ignition (LOI) of bulk dry sediment	MM	$mg.cm^{-3}$
	Concentration of organic matter from loss-on-ignition of bulk dry sediment	OM	$mg.cm^{-3}$
	Grain size particles from 0 to 2 μm	Clay	%
	Grain size particles from 2 to 20 μm	FineSilt	%
	Grain size particles from 20 to 50 μm	CoarseSilt	%
	Grain size particles from 50 to 200 μm	FineSand	%
	Grain size particles from 200 to 2000 μm	CoarseSand	%

Table 3
Outputs of the change point analyses (dates, expressed in cal BP) based on the mean (Mean) and on both the mean and variance (Mean + Var). Fixed maximum period of Q = 4, corresponding to 3 points changes are reported for the highest Akaike Information Criterion (AIC).

Variables	Mean based moments (cal BP)	Mean + Var based moments (cal BP)	Common dates (cal BP)
Clay	No change in mean	11,260; 10,379; 5530	–
Fine silt	10,760; 4873; 3141	10,411; 5878; 3141	3141
Coarse silt	10,411; 5914; 3141	10,411; 5914; 3141	10,411; 5914; 3141
Fine sand	8391; 7593; 5231	8361; 7593; 5231	8361; 7593; 5231
Coarse sand	10,411; 3169; 221	10,760; 3169; 208	3169
Organic Matter	10,348; 4567; 2055	4567; 3811; 2134	–
Mineral Matter	11,295; 10,348; 4400	11,226; 10,348; 4400	10,348; 4400

2.6. Plant macroremains-based vegetation reconstruction

For plant-cover estimates, the core was sampled every 1 cm, yielding 695 contiguous 1-cm thick samples (Leys et al., 2014). To characterize past vegetation, subfossil plant macroremains were preferred to pollen record that biases local vegetation pattern in mountain areas with sever relief due to long distance transport of pollen, notably of *Pinus* (Blarquez et al., 2013). Subfossil plant macroremains were identified and their abundances were expressed as accumulation rates (or influx) based on deposition time as computed by the age ~ depth model (fragments nb cm^{-2} yr^{-1}). Only plant macroremains whose abundance were greater

than 2% during the Holocene (11,650 years) were used for the analysis of interactions with sedimentological and fire variables. Accumulation rate of tree macroremains is a proxy of tree basal area or tree cover, since the higher the basal area, the more abundant the macroremains (Blarquez et al., 2012; graphical explanation in Fig. 1c).

The richness of plant macroremains was calculated following a rarefaction method appropriate for low abundances of bio- or geo-proxies and, takes into account the variability in deposition time resulting from the age ~ depth model (Blarquez et al., 2013). We used codes available here: http://paleoecologie.umontreal.ca/category/code/ to estimate taxonomic richness [$E(T_n)$] based on rarefaction analysis, following:

$$E(T_n) = \sum_{i=1}^{T} 1 - \left[\binom{N - N_i}{n} \Big/ \binom{N}{n} \right]$$

where *E(Tn)* is the rarefied taxonomic richness, N is the influx sum of particles in a sample, N_i is the influx of particles for the ith taxon, and n the minimum influx along a sedimentary record (Heck et al., 1975).

2.7. Statistical analyses

Z-score values were calculated to depict positive and negative deviations from the mean across the specified period for grain size categories. The data were centered and scaled using the scale function on the R base package. To determine the time periods presenting the most contrasting conditions for each sedimentological variable, change point analyses were performed on time series of clay, silts, sands, OM and MM. The change point analyses were based on mean, or on both mean and variance. For the analysis solely based on means, the function applied from the R package changepoint (v2.2.4, Killick and Eckley, 2014) was cpt.mean() with the SegNeigh method and AIC penalty. To conduct the analysis considering both mean and variance, the R function used was cpt.meanvar(). As this study specifically centers on the Holocene, during which interactions between fire and plant cover occurred, the time span for the change point analyses encompassed the series from 11,500 cal BP to present day.

Regarding the charcoal record, the statistical analyses resulted in the estimation of two of the three complementary components of the fire regime i.e., temporal component, spatial component (severity) and fire behavior (He et al., 2019). The FRI describes the temporal component of the fire regime, whereas the magnitude of $CHAR_{area}$ (or $CHAR_{conc}$) characterizes the local fire severity or burned area (schematized in Fig. 1b).

A multiple factor analysis (MFA; Escofier and Pages, 1994; Bécue-Bertaut and Pagès, 2008) was conducted to decipher the links among the different variables considered in the present study (Fig. 1d). The MFA is a symmetrical ordination based on correlation. This analysis was specifically chosen to ordinate the different variables (not assumed to be explanatory in the first place) with no risk of overfitting. Variables (Table 2) were grouped into three categories: sediment (7 variables), vegetation (4 variables), and fire (3 variables). The MFA was carried out using the MFA function from the FactoMineR package (Husson et al., 2007). The MFA outputs were plotted using the fviz_mfa() function from the factoextra package (Kassambara and Mundt, 2019). The quality of the representation (cos2) of each variable for the four first axes of the MFA, i.e. the proportion of the variable, were illustrated by each axis using the corrplot() function from the corrplot package (Wei et al., 2017). To analyze the relationships among the three groups of variables, the rhô-vectorial (RV) coefficients from the MFA were extracted, measuring the similarity (squared correlation) between each pair of groups, and expressed between 0 (minimum) and 1 (maximum). These coefficients were finally tested using the coeffRV() function from the FactoMineR package.

Generalized additive models (GAM) have been plotted on long term trends of sedimentology variables over time (Fig. 6 and S4). Linear regressions with adjusted R-squared and p-value were also performed between the FRI, the sedimentological individual variables and the plant rarefaction using the summary function on lm functions of the R basic package. The graphs showing the data points (Fig. 6 and S4), the line derived from the linear model and the confidence interval envelope around the line, were plotted with the ggplot2 package, geom-smooth (method = lm) function on R (Wickham, 2016).

3. Results

3.1. Dynamics of particle sizes, organic and mineral matter

The high-resolution chronology of z-scores of clays, silts and sands cover the Younger Dryas (YD) and Holocene, specifically from 12,250 cal BP to present (Figs. 3 and 4 and S3). Table 3 presents the significant change points determined from the clay, silt, sand, MM and OM contents. The moments of change points are plotted in Fig. 2 based on only the mean, or the mean plus the variance.

The Lateglacial and YD periods are marked by the highest z-score values for all grain sizes, on the positive side for clay and silt and negative for sand, except a small incursion into positive values of coarse sand during the Lateglacial/YD transition (Fig. S3). These periods are characterized by a very poor vegetation cover (no forest), and a lack of soil, or a non-mobilized soil. The fine particles constitute the main contribution to the lacustrine system. To better highlights the particle size pattern during the Holocene and reduce the magnitude of the y axis, we therefore plotted the values from 12,000 cal BP.

Clay, fine silt and coarse silt particles show similar trajectories with high z-scores from 11,500 to 10,400 cal BP, then low and rather steady values until ca. 5500 cal BP. From 3140 until today clay and silts display very high z-scores. The period between ca. 5900 and 3140 cal BP is intermediate and oscillating around the null values.

Fine and coarse sands present similar temporal patterns of z-scores, but differences can be observed (Fig. 3). First, coarse and fine sands increased from 11,500 cal BP to 10,700–10,400 cal BP, and then remained high until 8400 cal BP for fine sands and until 7500 cal BP for coarse sand but with a very noisy pattern. At ca 8400 cal BP, fine sands remain high, then dropped dramatically until 7600 cal BP, attaining their lowest Holocene values at 8250 cal BP. After the drop, fine sands start to recover presenting values similar to what they were before 8400 cal BP. This phase lasted 800 years and present an important similarity in terms of magnitude and duration with the pattern observed during the transition between the late YD and the early Holocene, from 12,250 to 10,750 cal BP (Fig. 4, Fig. S3). From 7600 to 5200 cal BP, the fine sands contents were on average high, then slightly decreased until today with a noisy pattern (Fig. 3). The coarse sands content was also high, but extremely noisy from 10,400–3200 cal BP. Values decreased slightly after 3200 cal BP, but in a noisy way that indicates high variability, reaching the lowest values between 2250 and 900 cal BP. The last 900 years presented a gentle uptrend, much steeper since 200 cal BP. The 8250 cal BP event was marked only recorded in terms of fine sands excursion between 8400 and 7600 cal BP (Fig. 4; Table 3).

To sum-up the multimillennial trends, clay and silt presented similar contrasts with those of sands (Fig. 3, Fig. S4). The only period in which fine sands did not behave as coarse sands was in a period surrounding the 8.2 kyr event (from 8400 to 7500 cal yr BP) where only fine sands dropped abruptly before rising progressively for 600 years (Fig. 4). Because of these similarities, the drivers that controlled the fine sands during the YD/Holocene transition and the 8.2-kyr event present common pattern between these two times suggesting common climatic features. On average, the first part of the Holocene (10,500–5900 cal BP) corresponds to high z-scores of sands, and the third part since (i.e., 3140 cal BP) presents high z-scores of clay and silt. The second part between 5900 and 3140 cal BP was transitory presenting values around 0, which

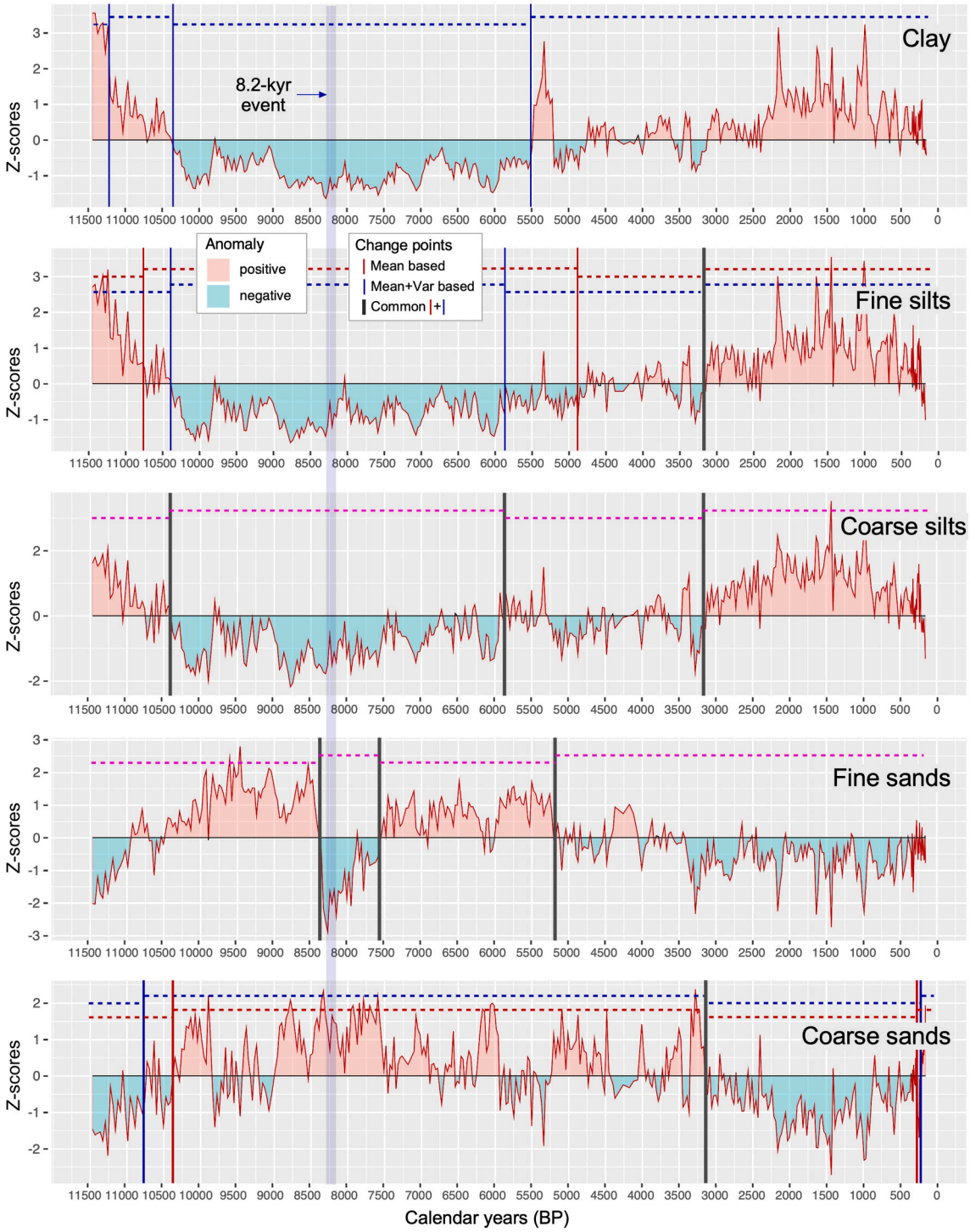

Fig. 3. Mineral matter fractions plotted against time. Data series have been transformed (z-scores) in order to preserve trends and compare data. The null value corresponds to the mean over the considered period.

is intermediate between the early and the late Holocene.

3.2. Relationships among fire, vegetation, and sediment variables

The multiple factor analysis, MFA (Fig. 5), shows that variables associated to sediments (i.e., organic matter, mineral matter, coarse and fine silts, and clay) were positively represented on the positive side of the axis 1, these variables were negatively correlated to both coarse and fine sands, as well as to the long fire return interval (FRI). The MFA axis 1 represents a gradient of precipitation and fire frequency. Important tree cover, fine sediment and organic content, and frequent fires are opposed to coarse silt and sand. The MFA revealed that charcoal accumulation rate values (CHARa and CHARc) were poorly correlated with vegetation and sediment variables, but moderately correlated to FRI. The second axis is driven by CHARa and CHARc, which is a gradient of fire severity or burned area. Variables of the vegetation group are poorly represented on the two first MFA axes, which capture 44.3% of the total data variability (Axis 1: 26.7%; Axis 2: 17.6%). The other three axes represent only 14.6, 9.6, and 8.1% of variance (Fig. 5) making them poorly informative. Vegetation variables, more specifically *Fagus* and

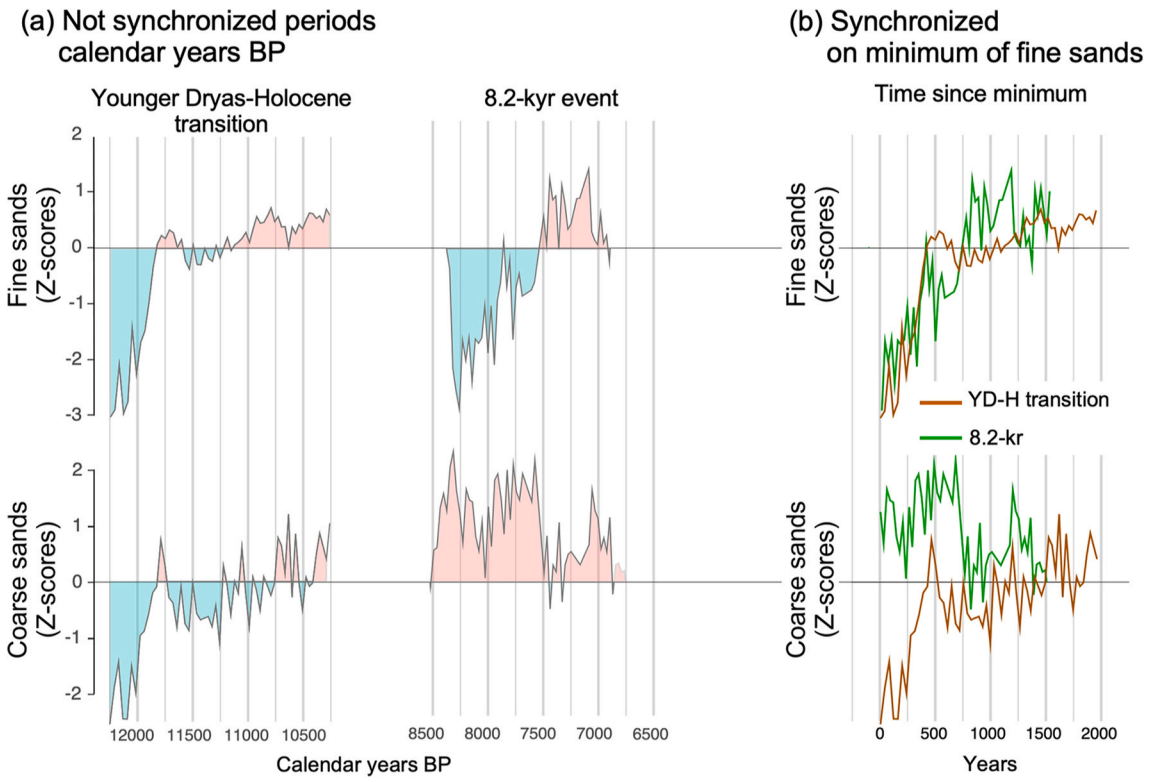

Fig. 4. Pattern of fine and coarse sands at the end of Younger Dryas and at the 8.2-kyr event, (**a**) as a function of time in calendar years BP, and (**b**) synchronized on the minimum values before the recovering phase. The Younger Dryas z-scores of all grain-sizes are presented in Figs. SI–2 that cover part of the Lateglacial (from 14,000 cal BP) to the early Holocene (9000 cal BP).

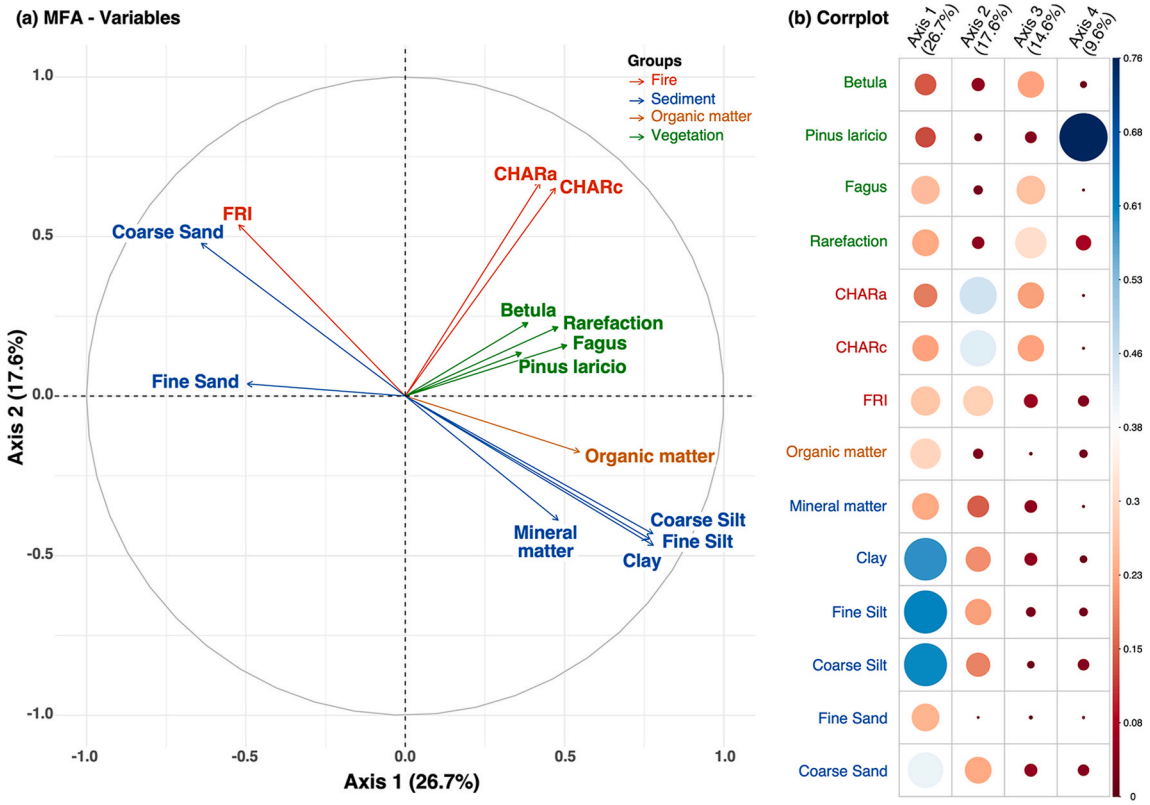

Fig. 5. Multiple factor analysis (MFA) for the three groups of variables: *Fire* (2 variables), *Sediment* (7 variables) and *Vegetation* (4 variables), as reported in Table 1. (**A**) Scatter plot of all variables in the two main axis; (B) corrplot of the first four axes, with their respective percentages, and the variables contributions for each axe. The size of the circle as well as the color range from red to blue is proportionate to the importance of the variable for the axis considered.

Betula were better correlated to axis 3, and *Pinus laricio* to axis 4 (Fig. 5).

The RV coefficients between groups (not illustrated) revealed the highest similarity of trends (15%) between fire and sediment variables, and the smallest between fire and vegetation variables (3%). The RV coefficient between vegetation and sediment variables was 7%, which is rather low. These RVs indicate that the best similarity between sediment and other environmental variables was found primarily for fire and secondly for vegetation.

3.3. Correlations between the FRI and particle size or plant richness

According to the results of the linear regressions (Fig. 6), the fire return intervals (FRI) were significantly correlated to the sediment variables ($p \leq 0.001$). A positive relation was found between FRI and fine and coarse sands, whereas the reverse was found for clay, fine silt and coarse silt particles, as well as MM and OM content. The longer the fire intervals, the more sands, and the less clay and silts. Plant richness (rarefaction) was the only variable that was not significantly correlated with FRI.

4. Discussion

The present study shows that frequent fires correlated well with accumulation of mineral matter (MM). In detail, this first concerns clay and silts sorted by lower intensity rainfall, and second, with MM content that reveals longer but mild rains. The vegetation composition represented by the abundance of pine, beech and birch was poorly correlated to sediment organic or mineral matter, as well as to the FRI and fire severity ($CHAR_{conc}$ or $CHAR_{area}$). These facts suggest there were no relationships between the tree-cover and erosion or fire occurrence. Sediment organic matter contents correlate well with FRI indicating significant litter inputs from the catchment supplying terrestrial organic matters to the lake and thus reducing the redox conditions. However, an increase in the lake productivity linked to nutrients brought by the vegetation combustion cannot be ruled out.

These findings partly support the hypothesis that fire and precipitation regime controlled multimillennial erosion trends. However, contrary to our assumption, vegetation had little aftermaths on mass erosion, and sand particles were not related with high fire frequency that would remove vegetation facilitating erosion. Instead, climate seems to be the main factor controlling fire frequency. Wetter climate had fostered erosion of sand particles (intense rainfall) and decreased the frequency of fires.

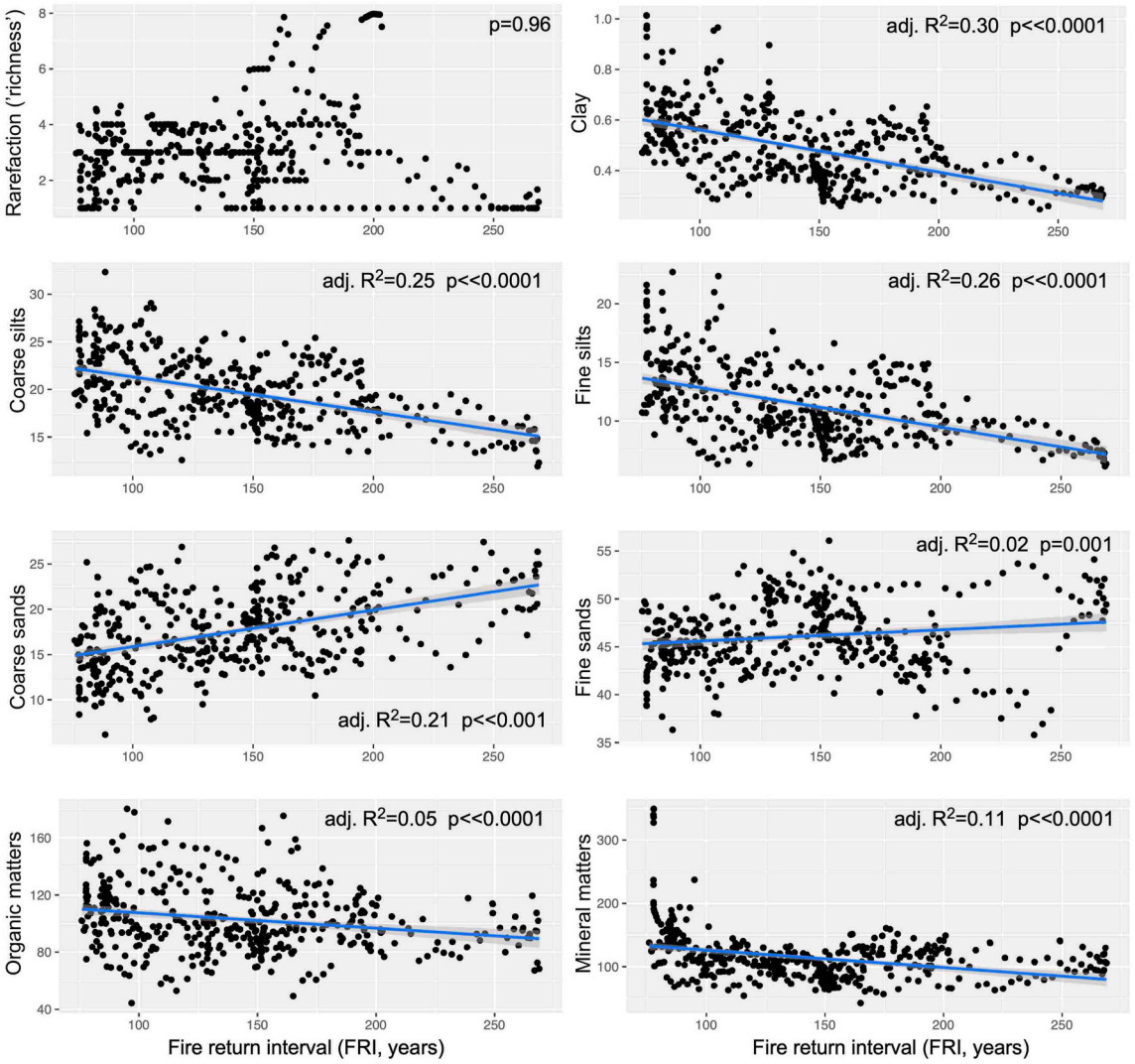

Fig. 6. Linear regression between plant richness (rarefaction), clay, fine and coarse silts, fine and coarse sands, mineral and organic matter contents and fire return intervals.

4.1. Wildfires and drier climate covary, driving fine particles erosion

The periods of high fire frequency (low FRI) correlated well with periods of inputs of clay and silts in the sediments, while periods of low fire frequency correlated with coarse sands (Fig. 6): the more fire, the more clay and silts were eroded, and conversely, the less frequent the fire, the more sand was eroded. This dipole suggests that the system is first and foremost top-down controlled by precipitation regimes. Wetter climate including high intensity rains yielded erosion of sands, mostly the coarse fraction, and reduced the occurrence of fire, while long drier periods favored fire occurrences and erosion of only clay and silts.

Changes in MM occurred during periods of short FRI (Fig. 6). This underscores that past fires were associated to erosion, as extensively evoked in the Mediterranean (e.g., Myronidis et al., 2010; Shakesby, 2011; Depountis et al., 2020; Stefanidis et al., 2022). The erosion of MM at Creno Lake supplied mainly clay and silts, which indicates that rains were not intense but probably lasted longer. However, this past observation-based output contradicts with model-based output that suggest erosion is linked to the amount and intensity of rain rather than the number of precipitation days (Nearing et al., 2004). The role of fire on erosion of clay and silts might be explained by the consumption of soil organic matters (e.g., Mirzaei et al., 2023) that binds mineral particles and elements thus leading to a destruction of soil aggregates, a reduction of soil hydrophobia, and an increase in soil bulk density (Roshan and Biswas, 2023). After fires, these particles are free, more hygrophilous and more likely to be mobilized by even low intensity rainfalls.

Organic matters (OM) appear partly linked to the vegetation cover, plant macroremains of *Pinus*, *Fagus* and *Betula*, since they were all driven on the MFA-1 (Fig. 5). Surprisingly, the OM content increases in sediments when fires are more frequent (Fig. 6, $p \ll 0.0001$). One could assume this increase result from post-fire erosion of terrestrial OM. However, fire probably released nutrients such as P, K, Ca, Mg from biomass combustion (Roshan and Biswas, 2023), thus changing the in-lake productivity of algae. Commonly, these elements are poorly recycled in lakes due to sequestration in sediments, making this terrestrial influx potentially useful to pulse lake productivity. However, it seems that lakes would be buffered or resilient to the nutrient fluxes associated with single fires (e.g., Lewis et al., 2004), but could be affected by the fire severity or frequency (Waters et al., 2019), which enhance the nutrient fluxes once in case of severity or repetitively for frequency. Overall, the OM increase associated with short fire intervals seems more related to erosion of litter and humus from the fire-associated lake area, but an increase in the lake productivity as a response to fire cannot be excluded.

Finally, infrequent fires occurred when fine and coarse sands chiefly accumulated in sediments. This indicates that during periods characterized by intense rain/runoff, fires were less frequent, and the climate was likely wetter. However, despite our assumption, fire severity reported by $CHAR_{conc}$ or $CHAR_{area}$ presents no links with fire frequency nor with clay influx reporting dryness. Interestingly, years of severe fires during 20th century have been driven by heat waves and dryness (Şahan et al., 2022) supporting simulations for the 21st century (Turco et al., 2018; Ruffault et al., 2020). This suggest that recent years could have disrupted with the long range of variability reported in the present study.

4.2. Precipitation trends over the Holocene

Clay covaries with fine and coarse silts over the Holocene, whereas fine and coarse sands present opposite trends. Intense rainfalls favor transport of large particles, like coarse and fine sands (Kinnel, 1976; Fernández-Raga et al., 2017), whereas the total sediment yield (MM) depends on the rain duration (Sun et al., 2021). Based on these allometry, the early Holocene from about 10,500 cal BP would be marked by a high rain intensity that transported abundantly coarse and fine sands (Fig. 4). The intense rainfalls decreased throughout the Holocene, but more rapidly from 3200 cal BP for very intense rainfalls according to coarse sands (Fig. S4). This observation indicates that the early Holocene experienced more intense rains than the late-Holocene, and that the change took place progressively after 10,500 cal BP. The sole exception corresponds to the 8.2 kyr event that is an anomaly in the multimillennial trends. Paleo-floods study from the Alps in diverse environmental conditions indicates that heavy spring and winter flooding result from precipitation events and the rapid melting of snow (Kämpf et al., 2014), a phenomenon that could also have happened at our study site.

The period of lowest rain intensity began at 3200 cal BP since fine and coarse silts, and lasted until 200 cal BP (late 18th century). Interestingly, around 5000 and 3200 cal BP, the sedimentological sequence was extremely steady for all grain-sizes, contrasting with the hypothesize of a dry event that would have occurred around 4200 cal BP in the Mediterranean basin (Bini et al., 2019). This 4200-event is well reported further east both in the Near-East (Bar-Matthews et al., 1997; Arz et al., 2006; Parker et al., 2006) and further south in the African tropical areas (Gasse and Van Campo, 1994; Thompson et al., 2002), but remains disputed in the west Mediterranean basin.

Clay and silts covary with MM (Fig. 5), and present a rising trend during the second half of the Holocene (Fig. S4). This suggests that intense rains decreased progressively during the Holocene, mainly during the last 3000 years. The exception is the past 300 years (200 cal BP to present) when more intense rainfalls probably occurred as revealed by the dominance sands, chiefly the coarse ones. The increase in clay over the late Holocene is a common pattern with other studies in the northwestern Mediterranean basin (e.g., Sabatier et al., 2020; Goutiers and Carcaillet, 2022), which was inferred to Saharan 'red' rains based on mineralogical analyses of different fractions of clay combined with a geographic model of earth element signatures (Sabatier et al., 2020). Indeed, Saharan atmospheric inputs were a dominant process in Corsica since 3100 years at least, and increased since ca 1070 years (Sabatier et al., 2020), with modern potential deposition rate of more than 10 tons.km^{-2}.yr^{-1} (Loye-Pilot et al., 1986). Such atmospheric inputs can have important aftermath on the nutrient budgets of mountain ecosystem (Loye-Pilot and Morelli, 1988; Aciego et al., 2016), considering the contribution of P, K, Ca and Mg (Loye-Pilot et al., 1986; Cortizas et al., 2019; Goutiers and Carcaillet, 2022). In summary, the clay inputs to the sediments would therefore be indirect because they do not result from in situ weathering of the bedrock (monzonic granite) but from Saharan atmospheric inputs, modulated both by the precipitation regime and the frequency of fires.

4.3. Precipitation trends and the 8.2-kyr event: fine and coarse sands' signature

The main abrupt anomaly during the Holocene concerns fine sands only, that dropped from 8400 to 8200 cal BP, coinciding with the 8.2 kyr climatic event, which was a rapid cooling event (2–4 °C according to Kobashi et al., 2007; 1 °C according to Morrill et al., 2013) that occurred chiefly in North-Atlantic areas (Morrill et al., 2013; Parker and Harrison, 2022). The drop in fine sands lasted less than 200 years (Fig. 3). The exact date of the drop and its duration depends on the quality of the age∼depth model. The duration could have been shorter as reported by Parker and Harrison (2022). Whatever the accuracy of the duration, this drop reveals a change in the precipitation pattern or seasonality.

The 8.2 kyr event was a drier period on average (less fine sands) with high rain intensity or short-lasting runoff, strong enough to mainly sort coarse sands that remained high. The system returned to its initial state in about 600 years (Fig. 4), i.e., ending at 7600 cal BP. This terminal date, 7600 cal BP is closed to recent assessment of 7900 cal BP (Parker and Harrison, 2022). Interestingly, Morrill et al. (2013) reported different climatic patterns during the 8.2 kyr according to proxies and archives used for climatic reconstructions, and selected areas. Indeed,

pollen-based reconstruction would characterize an event with drier years on average, whilst speleothem-based reconstruction would reveal higher spring runoff due to snow melting in mountain areas (Parker and Harrison, 2022). Our outputs align perfectly with this described scenario, pointing to elevated short-term precipitation or runoff during a drier period on average. Furthermore, the elevation of Creno Lake (1310 m asl) which peaks over 1500 m asl on a west-facing mountain slope (wetter) strongly pleads for this second scenario of high spring runoff strengthened by snowy winters during colder and drier years.

If the 8.2 kyr event would have been drier with spring runoff due to snow melting, the comparison with YD (Fig. 4) reveals the difference between these two periods. The YD would have also been dry on average but without effect of runoff supplying coarse sands. Because YD was a well-known cold period, winter snow cover was certain, but probably too thin to trigger spring runoff needed to transport coarse sands.

Interestingly the recovery after 8200 cal BP occurred in a similar duration as in the late YD (Fig. 4). This similarity suggests that both periods present certain common characteristics: cold and dry. However, both periods differed by the patterns of coarse sands that were very low during the YD compared to the 8.2 kyr event. Based on grain sizes patterns, the YD in Corsica would have been characterized by less precipitation than the 8.2 kyr event, without runoff that lasted between 12,600 and 11,300 cal BP (Fig. S3). The high influx of coarse sands during the beginning of the YD, i.e., between 12,900 and 12,600 cal BP (Fig. S3), indicates a runoff period, may be related to winter snow precipitation followed by spring runoff, like during the 8.2 kyr event.

However, the tree-cover of the YD was lower than that of the 8.2 kyr event therefore changing the pattern of particles transportation to the lake whatever the precipitation regime. The first tree occurrences around the lake – based on *Pinus nigra* needles – are dated to 13,200 cal BP, and tree-cover rose until 12,000 cal BP (Leys et al., 2014). Comparatively, at 8300 cal BP, the slopes around the lake were covered by a mixed *Pinus laricio-Fagus sylvatica* cover (Leys et al., 2014), which probably protected the fine sand fraction of soil from erosion.

5. Conclusion

High fire frequency (short intervals) were associated with erosion of clay, silt, and organic and total mineral matter. Conversely, low fire frequency (long intervals) correlate well with the transport of sands, mainly the coarse fraction. The system appears top-down controlled by climate driving both fire regimes, erosion and the sorting of particle size, although fires can also drive sediment patterns by its own. The vegetation cover did not affect sediment variations. The 200-yr and over abrupt drop in fine sands at the 8.2-kyr event suggests a severe drought, followed by about 600 years until ecosystem recover in terms of climate, fire and tree-cover. Overall, the early Holocene (from 10,700 to 7500 cal BP) was very humid, whereas the late Holocene (from 3200 to 200 cal BP) was drier. Between 7500 and 3200 cal BP, the precipitation regime was intermediate. The past 900 years have been characterised by a progressive increasing runoff dragging more sands.

Ethics approval and consent to participate

Not applicable.

Consent for publication

Not applicable.

Funding

Financial support was provided by the FIREMAN program (ERA-net BiodivERsA, ANR-08-BDVA-0004) to CC and by a PhD grant to BL from the Ecole Pratique des Hautes Etudes (EPHE-PSL). This study contributes to the International Emerging Action MedFires to CC (CNRS CoopIntEER IEA00797). CC is indebted to Churchill College in Cambridge and the French Embassy in London for their support as By-Fellow during the writing of the article.

Declaration of competing interest

The authors declare that they have no known competing financial interests or personal relationships that could have appeared to influence the work reported in this paper.

Data availability

Data will be made available on request.

Acknowledgements

For their help during the fieldwork, we thank Loïc Bircker, Olivier Blarquez, Laurent Bremond, Benoit Brossier, Thomas Fournier and Gina Hannon. We are grateful to field rangers of the Regional Natural Park of Corsica for their advice to organize the fieldwork using mules.

Appendix A. Supplementary data

Supplementary data to this article can be found online at https://doi.org/10.1016/j.quascirev.2024.108602.

References

Aciego, S.M., Riebe, C.S., Hart, S.C., Blakowski, M.A., Carey, C.J., Aarons, S.M., Dove, N. C., Botthoff, J.K., Sims, K.W.W., Aronson, E.L., 2016. Dust outpaces bedrock in nutrient supply to montane forest ecosystems. Nat. Commun. 8, 14800 https://doi.org/10.1038/ncomms14800.

Aleman, J.C., Blarquez, O., Bentaleb, I., Bonté, P., Brossier, B., Carcaillet, C., Gond, V., Gourlet-Fleury, S., Kpolita, A., Lefèvre, I., Oslisly, R., Power, M.J., Yongo, O., Bremond, L., Favier, C., 2013. Tracking land-uses with sedimentary charcoals in tropics. Holocene 23, 1853–1862. https://doi.org/10.1177/0959683613508159.

Arz, H.W., Lamy, F., Pätzold, J., 2006. A pronounced dry event recorded around 4.2 ka in brine sediments from the northern Red Sea. Quat. Res. 66, 432–441.

Badeau, J., Guibal, F., Fulé, P.Z., Chauchard, S., Moneglia, P., Carcaillet, C., 2024. 202 years of changes in Mediterranean fire regime in *Pinus nigra* forest. Corsica. For. Ecol. Manag. 554, 121658 https://doi.org/10.1016/j.foreco.2023.121658.

Bar-Matthews, M., Ayalon, A., Kaufman, A., 1997. Late quaternary paleoclimate in the eastern mediterranean region from stable isotope analysis of speleothems at soreq cave, Israel. Quat. Res. 47, 155–168.

Bécue-Bertaut, M., Pagès, J., 2008. Multiple factor analysis and clustering of a mixture of quantitative, categorical and frequency data. Comput. Stat. Data Anal. 52, 3255–3268.

Bini, M., Zanchetta, G., Persoiu, P., Cartier, R., Català, A., Cacho, I., Dean, J.R., Di Rita, F., Drysdale, R.N., Finnè, M., Isola, I., Jalali, B., Lirer, F., Magri, D., Masi, A., Marks, L., Mercuri, A.M., Peyron, O., Sadori, L., Sicre, M.A., Welc, F., Zielhofer, C., Brisset, E., 2019. The 4.2 kaBP Event in the Mediterranean region: an overview. Clim. Past 15, 555–577. https://doi.org/10.5194/cp-15-555-2019.

Blaauw, M., Christen, J.A., 2011. Flexible paleoclimate age-depth models using an autoregressive gamma process. Bayesian Anal 6, 457–474. https://doi.org/10.1214/11-BA618.

Blarquez, O., Carcaillet, C., Elzein, T.M., Roiron, P., 2012. Needle accumulation rate model-based reconstruction of palaeo-tree biomass in the western subalpine Alps. Holocene 22, 579–587. https://doi.org/10.1177/0959683611427333.

Blarquez, O., Finsinger, W., Carcaillet, C., 2013. Assessing paleo-biodiversity using low proxy influx. PLoS One 8, e65852. https://doi.org/10.1371/journal.pone.0065852.

Carcaillet, C., Perroux, A.S., Genries, A., Perrette, Y., 2007. Sedimentary charcoal pattern in a karstic underground lake, Vercors massif, French Alps: implications for palaeo-fire history. Holocene 17, 845–850. https://doi.org/10.1177/0959683607080526.

Christopoulou, A., Fulé, P.Z., Andriopoulos, P., Sarris, D., Arianoutsou, M., 2013. Dendrochronology-based fire history of *Pinus nigra* forests in mount taygetos, southern Greece. For. Ecol. Manage. 293, 132–139. https://doi.org/10.1016/j.foreco.2012.12.048.

Cisnero, M., Cacho, I., Moreno, A., Stoll, H., Torner, J., Catala, A., Edwards, R.L., Cheng, H., Fornos, J.J., 2021. Hydroclimate variability during the last 2700 years based on stalagmite multi-proxy records in the central-western Mediterranean. Quat. Sci. Rev. 269, 107137 https://doi.org/10.1016/j.quascirev.2021.107137.

Clark, J.S., Lynch, J., Stocks, B.J., Goldammer, J.G., 1998. Relationships between charcoal particles in air and sediments in west-central Siberia. Holocene 8, 19–29.

Cortizas, A.M., López-Costas, O., Orme, L., Mighall, T., Kylander, M.E., Bindler, R., Sala, G., 2019. Holocene atmospheric dust deposition in NW Spain. Holocene 30, 507–518.

Day, P.R., 1965. Particle fractionation and particle-size analysis. In: Black, C.A. (Ed.), Methods of Soils Analysis: Part 1 Physical and Mineralogical Properties, Including Statistics of Measurements and Sampling, 9.1. American Society of Agronomy, Madison, pp. 545–567. https://doi.org/10.2134/agronmonogr9.1.c43.
Depountis, N., Michalopoulou, M., Kavoura, K., Nikolakopoulos, K., Sabatakakis, N., 2020. Estimating soil erosion rate changes in areas affected by wildfires. ISPRS Int. J. Geo-Inf. 9, 562. https://doi.org/10.3390/ijgi9100562.
Escofier, B., Pages, J., 1994. Multiple factor analysis (AFMULT package). Comput. Stat. Data Anal. 18, 121–140.
Fernandez-Guisuraga, J.M., Calvo, L., 2023. Fuel build-up promotes an increase in fire severity of reburned areas in fire-prone ecosystems of the western Mediterranean. Fire Ecol 19, 72. https://doi.org/10.1186/s42408-023-00232-0.
Fernández-Raga, M., Palencia, C., Keesstra, S., Jordán, A., Fraile, R., Angulo-Martínez, M., Cerdà, A., 2017. Splash erosion: a review with unanswered questions. Earth Sci. Rev. 171, 463–477. https://doi.org/10.1016/j.earscirev.2017.06.009.
Fulé, P.Z., Ribas, M., Gutiérrez, E., Vallejo, R., Kaye, M.W., 2008. Forest structure and fire history in an old *Pinus nigra* forest, eastern Spain. For. Ecol. Manag. 255, 1234–1242. https://doi.org/10.1016/j.foreco.2007.10.046.
Gamisans, J., Badia, J.N., Rafols, E.S., 2000. La Végétation de la Corse. Edisud, p. 391.
Gasse, F., Van Campo, E., 1994. Abrupt post-glacial climate events in West Asia and North Africa monsoon domains. Earth Planet Sci. Lett. 126, 435–456.
Goutiers, V., Carcaillet, C., 2022. Geochemistry and sedimentology of a minerotrophic peat in a western Mediterranean mountain wilderness area. Quaternary 5, 48. https://doi.org/10.3390/quat5040048.
He, T., Lamont, B.B., Pausas, J.G., 2019. Fire as a key driver of Earth's biodiversity. Biol. Rev. 94, 1983–2010. https://doi.org/10.1111/brv.12544.
Heck, K.L.Jr, van Belle, G., Simberloff, D., 1975. Explicit calculation of the rarefaction diversity measurement and the determination of sufficient sample size. Ecology 56, 1459–1461. https://doi.org/10.2307/1934716.
Hennebelle, A., Aleman, J.C., Ali, A.A., Bergeron, Y., Carcaillet, C., Grondin, P., Landry, J., Blarquez, O., 2020. The reconstruction of burned area and fire severity using charcoal from boreal lake sediments. Holocene 30, 1400–1409. https://doi.org/10.1177/0959683620932979.
Higuera, P.E., Whitlock, C., Gage, J.A., 2011. Linking tree-ring and sediment-charcoal records to reconstruct fire occurrence and area burned in subalpine forests of Yellowstone National Park, USA. Holocene 21, 327–341.
Husson, F., Josse, J., Lê, S., Mazet, J., 2007. Factor Analysis and Data Mining with R. FactoMineR Package.
IFN, 2006. Inventaire forestier départemental Haute-Corse (2004) et Corse-du-Sud (2003); 3e inventaire. Inventaire Forestier National, France. https://inventaire-foretier.ign.fr/IMG/pdf/IFN_20_3_CORSE.pdf.
Kämpf, L., Brauer, A., Swierczynski, T., Czymzik, M., Mueller, P., Dulski, P., 2014. Processes of flood-triggered detrital layer deposition in the varved Lake Mondsee sediment record revealed by a dual calibration approach. J. Quat. Sci. 29, 475–486.
Kassambara, A., Mundt, F., 2019. Factoextra: extract and visualize the results of multivariate data analyses. R package version 1.0. 5., 2017
Killick, R., Eckley, I.A., 2014. Changepoint: an R package for changepoint analysis. J. Stat. Softw. 58, 1–19. https://doi.org/10.18637/jss.v058.i03.
Kinnel, P.I.A., 1976. Splash erosion of primary particles and aggregates. Soil Sci. Soc. Am. J. 40, 966–968. https://doi.org/10.2136/sssaj1976.03615995004000060044x.
Kobashi, T., Severinghaus, J.P., Brook, E.J., Barnola, J.M., Grachev, A.M., 2007. Precise timing and characterization of abrupt climate change 8,200 years ago from air trapped in polar ice. Quat. Sci. Rev. 26, 1212–1222.
Lewis, T.L., Lindberg, M.S., Schmutz, J.A., Bertram, M.R., 2004. Multi-trophic resilience of boreal lake ecosystems to forest fires. Ecology 95, 1253–1263.
Leys, B., Carcaillet, C., Dezileau, L., Ali, A.A., Bradshaw, R.H.W., 2013. A comparison of charcoal measurements for reconstruction of Mediterranean paleo-fire frequency in the mountains of Corsica. Quat. Res. 79, 337–349. https://doi.org/10.1016/j.yqres.2013.01.003.
Leys, B., Finsinger, W., Carcaillet, C., 2014. Historical range of fire frequency is not the Achilles' heel of the Corsican black pine ecosystem. J. Ecol. 102, 381–395. https://doi.org/10.1111/1365-2745.12207.
Loye-Pilot, M.D., Morelli, J., 1988. Fluctuations of ionic composition of precipitations collected in Corsica related to changes in the origins of incoming aerosols. J. Aerosol Sci. 19, 577–585.
Loye-Pilot, M.D., Martin, J.M., Morelli, J., 1986. Influence of saharan dust on the rain acidity and atmospheric input to the mediterranean. Nature 321, 427–428. https://doi.org/10.1038/321427a0.
Lüning, S., Schulte, L., Garcés-Pastor, S., Danladi, I.B., Galka, M., 2019. The medieval climate anomaly in the mediterranean region. Paleoceanogr. Paleoclim. 34, 1625–1649. https://doi.org/10.1029/2019PA003734.
Lynch, J.A., Clark, J.S., Stocks, B.J., 2004. Charcoal production, dispersal, and deposition from the Fort Providence experimental fire: interpreting fire regimes from charcoal records in boreal forests. Can. J. For. Res. 34, 1642–1656.
Martinez-Cortizas, A., Lopez-Costas, O., Orme, L., Mighall, T., Kylander, M.E., Bindler, R., Gallego-Sala, A., 2019. Holocene atmospheric dust deposition in NW Spain. Holocene 30, 507–518. https://doi.org/10.1177/0959683619875193.
Merganič, J., Dudáková, Z., Merganičová, K., Vičková, M., Ferenčik, M., Jusko, V., Allman, M., 2023. Impact of fine woody debris on surface water run-off. Eur J Forest Res. https://doi.org/10.1007/s10342-022-01528-7.
Michalet, R., Choler, P., Callaway, R.M., Whitham, T.G., 2020. Rainfall continentality, via the winter Gams angl, provides a new dimension biogeographical distributions in the western United States. Global Ecol. Biogeogr. 30, 384–397. https://doi.org/10.1111/geb.13223.
Mirzaei, J., Heydari, M., Omidipour, R., Jafarian, N., Carcaillet, C., 2023. Decrease in soil functionalities and herbs' diversity, but not that of arbuscular mycorrhizal fungi, linked to short fire interval in semi-arid oak forest ecosystem, west Iran. Plants 12, 1112. https://doi.org/10.3390/plants12051112.
Moritz, M.A., Batllori, E., Bradstock, R.A., Gill, M., Handmer, J., Hessburg, P.F., Leonard, J., Mccaffrey, S., Odion, D.C., Schoennagel, T., Syphard, D.A., 2014. Learning to coexist with wildfire. Nature 515, 58–66. https://doi.org/10.1038/nature13946.
Morrill, C., Anderson, D.M., Bauer, B.A., Buckner, R., Gille, E.P., Gross, W.S., Hartman, M., Shah, A., 2013. Proxy benchmarks for intercomparison of 8.2 ka simulations. Clim. Past 9, 423–432. https://doi.org/10.5194/cp-9-423-2013, 2013.
Myronidis, D.I., Emmanouloudis, D.A., Mitsopoulos, I.A., et al., 2010. Soil erosion potential after fire and rehabilitation treatments in Greece. Environ. Model. Assess. 15, 239–250. https://doi.org/10.1007/s10666-009-9199-1.
Nearing, M.A., Pruski, F.F., O'neal, M.R., 2004. Expected climate change impacts on soil erosion rates: a review. J. Soil Water Conserv. 59, 43–50.
Nguyen, V.B., Nguyen, Q.B., Zhang, Y.W., Lim, C.Y.H., Khoo, B.C., 2016. Effect of particle size on erosion characteristics. Wear 348–349, 126–137. https://doi.org/10.1016/j.wear.2015.12.003.
Ohlson, M., Tryterud, E., 2000. Interpretation of the charcoal record in forest soils: forest fires and their production and deposition of macroscopic charcoal. Holocene 10, 519–525.
Parker, S.E., Harrison, S.P., 2022. The timing, duration and magnitude of the 8.2 ka event in global speleothem records. Sci. Rep. 12, 10542 https://doi.org/10.1038/s41598-022-14684-y.
Parker, A.G., Goudie, A.S., White, K., Hodson, M.J., Manning, M., Kennet, D., 2006. A record of Holocene climate change from lake geochemical analysis in southeastern Arabia. Quat. Res. 66, 465–476.
Pausas, J.G., Fernández-Muñoz, S., 2012. Fire regime changes in the Western Mediterranean Basin: from fuel-limited to drought-driven fire regime Clim. Change 110, 215–226. https://doi.org/10.1007/s10584-011-0060-6.
Reille, M., Gamisans, J., Andrieu-Ponel, V., de Beaulieu, J.L., 1999. The Holocene at Lac de Creno, Corsica, France: a key site for the whole island. New Phytol 141, 291–307.
Reille, M., Gamisans, J., de Beaulieu, J.L., Andrieu, V., 1997. The late-glacial at Lac de Creno (Corsica, France): A key site in the western Mediterranean Basin. New Phytol 135, 547–559.
Reimer, P.J., Austin, W.E.N., Bard, E., Bayliss, A., Blackwell, P.G., Ramsey, C.B., Butzin, M., Cheng, H., Edwards, R.L., Friedrich, M., et al., 2020. The IntCal20 Northern Hemisphere Radiocarbon Age Calibration Curve (0–55 cal kBP). Radiocarbon 62, 725–757. https://doi.org/10.1017/RDC.2020.41.
Riera, P., Peñuelas, J., Farreras, V., Estiarte, M., 2007. Valuation of climate-change effects on mediterranean shrublands. Ecol. Appl. 17, 91–100.
Rogers, B.M., Balch, J.K., Goetz, S.J., Lehmann, C.E.R., Turetsky, M., 2020. Focus on changing fire regimes: interactions with climate,ecosystems, and society. Environ. Res. Lett. 15, 030201 https://doi.org/10.1088/1748-9326/ab6d3a.
Roshan, A., Biswas, A., 2023. Fire-induced geochemical changes in soil: implication for the element cycling. Sci. Tot. Envir. 868, 161714 https://doi.org/10.1016/j.scitotenv.2023.161714.
Ruffault, H., Curt, T., Moron, V., Trigo, T.M., Mouillot, M., Koutsias, N., Pimont, F., Martin-StPaul, N., Barbero, R., Dupuy, J.L., Russo, A., Belhadj-Khedher, C., 2020. Increased likelihood of heat-induced large wildfires in the Mediterranean Basin. Sci. Rep. 10, 13790 https://doi.org/10.1038/s41598-020-70069-z.
Sabatier, P., Nicolle, M., Piot, C., Colin, C., Debret, M., et al., 2020. Past African dust inputs in the western Mediterranean area controlled by the complex interaction between the Intertropical Convergence Zone, the North Atlantic Oscillation, and total solar irradiance. Clim. Past 16, 283–298 ff10.5194/cp-16-283-2020.
Şahan, E., Köse, N., Güner, T., Trouet, V., Tavsanoglu, Ç., Akkemik, Ü., Dalfes, N., 2022. Multi-century spatiotemporal patterns of fire history in black pine forests, Turkey. For. Ecol. Manage. 518, 120296 https://doi.org/10.1016/j.foreco.2022.120296.
Sayedi, S.S., Abbott, B.W., Vanniere, B., Leys, B., Colombaroli, D., Gil Romera, G., Slowinski, M., Aleman, J.C., Blarquez, O., Feurdean, A., et al., 2024. Assessing changes in global fire regimes. Fire Ecol 20, 18. https://doi.org/10.1186/s42408-023-00237-9.
Shakesby, R.A., 2011. Post-wildfire soil erosion in the Mediterranean: review and future research directions. Earth-Science Rev. 105, 71–100.
Shi, X.H., Yue, B.J., Wang, L., Fang, N.F., Wang, D., Wu, F.Z., 2013. Effects of mulch cover rate on interrill erosion processes and the size selectivity of eroded sediment on steep slopes. Soil Sci. Society Am. J. 77, 257–267.
Stefanidis, S., Alexandridis, V., Spalevic, V., Mincato, R.L., 2022. Wildfire effects on soil erosion dynamics: the case of 2021 megafires in Greece. Agric. For. i Sumar. 68.
Sun, L., Zhou, J.L., Cai, Q., Liu, S., Xiao, J., 2021. Comparing surface erosion processes in four soils from the Loess Plateau under extreme rainfall events. Int. Soil Water Cons. Res. 9, 520–531. https://doi.org/10.1016/j.iswcr.2021.06.008.
Thompson, L.G., Mosley-Thompson, E., Davis, M.E., Henderson, K.A., Brecher, H.H., Zagorodnov, V.S., Mashiotta, T.A., Lin, P.N., Mikhalenko, V.N., Hardy, D.R., Beer, J., 2002. Kilimanjaro ice core records evidence of Holocene climate change in tropical africa. Science 298, 589–593.
Turco, M., Rosa-Cánovas, J.J., Bedia, J., Jerez, S., Montávez, J.P., Llasat, M.C., Provenzale, A., 2018. Exacerbated fires in Mediterranean Europe due to anthropogenic warming projected with nonstationary climate-fire models. Nat. Commun. 9, 3821. https://doi.org/10.1038/s41467-018-06358-z.
Walker, M., Johnsen, S., Rasmussen, S.O., Popp, T., Steffensen, J.P., Gibbard, P., Gibbard, P., Hoek, W., Lowe, J., Andrews, J., Bjorck, S., Cwynar, L.C., Hughen, K., Kershaw, P., Kromer, B., Litt, T., Lowe, D.J., Nakagawa, T., Newnham, R., Schwander, J., 2009. Formal definition and dating of the GSSP (Global Stratotype Section and Point) for the base of the Holocene using the Greenland NGRIP ice core, and selected auxiliary records. J. Quat. Sci. 24, 3–17.

Waters, M.N., Metz, A.P., Smoak, J.M., et al., 2019. Chronic prescribed burning alters nutrient deposition and sediment stoichiometry in a lake ecosystem. Ambio 48, 672–682. https://doi.org/10.1007/s13280-018-1094-z.

Wei, T., Simko, V., Levy, M., Xie, Y., Jin, Y., Zemla, J., 2017. Package 'corrplot.'. Statistician 56, 316–324.

Wickham, H., 2016. ggplot2: Elegant Graphics for Data Analysis. Springer.